



---

# Innovative form-finding method and modeling platform for cable dome design

Yan Zhou\*, Mingzhe Ma, Yaozhi Luo

\* College of Civil Engineering and Architecture, Zhejiang University, Hangzhou, Zhejiang, China  
zhouyan98@zju.edu.cn

## Abstract

This paper introduces an efficient form-finding method and a dedicated modeling and computational platform to enhance the efficiency of cable dome structure design. The form-finding method adopts a basic strategy by transforming nonlinear equilibrium equations into nonlinear least-squares problems and subsequently employing the improved Dog-Leg method to solve the transformed problems. The proposed method is highly efficient, capable of saving a significant amount of time in the analytical process, while the platform is designed to streamline the intricate modeling process. Comprising three modules, namely the pre-processing module, the computational module, and the post-processing module, the platform offers comprehensive support. The pre-processing module focuses on swift modeling of cable dome structures, setting material parameters, defining section parameters, establishing constraints, and applying loads. The computational module is capable of addressing various challenges, including prestress design, section design, static analysis, modal analysis, and dynamic analysis. The post-processing module allows for data analysis and visualization of computational results. The integration of the form-finding method within the platform proves instrumental in saving considerable time for engineers engaged in the design of cable dome structure.

**Keywords:** cable dome, tensegrity, form-finding, modeling platform, dog-leg method

## 1. Introduction

The cable dome structure, a typical non-self-stressed tensegrity structure, finds extensive application in the realm of long-span structures. The first and most renowned cable dome structure was proposed by Geiger [1], with representative projects including the 1986 Seoul Olympics gymnastics and the Suncoast Dome in the United States [2]. Another example of a typical cable dome structure is the Levy dome. In contrast to the Geiger dome, the Levy dome features a greater number of interconnected elements, resulting in enhanced overall stability. Notable projects showcasing this design include the Georgia Dome, which was completed in 1999 [3].

In tensegrity structure design, form-finding stands as a pivotal phase. It revolves around determining optimal prestress distributions and node coordinates within specified structural topology constraints, aiming to attain a stable equilibrium state. For tensegrity structures with boundary constraints, like cable domes, form-finding is also essential in the design process. Since the internal forces of tensegrity structures are highly related to their geometric configurations, form finding is a highly nonlinear problem. To address this challenge, extensive research has been undertaken, leading to the development of diverse form-finding methods.

Despite the strides made in form-finding methods, there remain constraints regarding methods incorporate physical information of structural elements. This is particularly relevant for tensegrity structures like cable domes, where analyzing equilibrium states under external forces and determining internal member forces are critical for engineering design. Additionally, the presence of kinematic modes in tensegrity structures can lead to singularities in stiffness matrices [4], which poses difficulties in solving nonlinear equations using the finite element method. To this end, this paper introduces an

innovative form-finding method for tensegrity structures, based on the improved Dog-Leg method. Initially, the nonlinear equilibrium equations of tensegrity structures are reformulated into nonlinear least-squares problems. To address this, the Dog-Leg method [5], a hybrid method of Gauss-Newton and steepest descent methods, is employed. While effective within a predefined trust region, this method may encounter issues with singular stiffness matrices. Consequently, the MBFGS (Modified Broyden-Fletcher-Goldfarb-Shanno) method [6], an improved version of the BFGS approach, is subsequently utilized. The resulting DL-MBFGS form-finding method demonstrates superior performance in handling stiffness matrix singularities. Ultimately, this form-finding method is applied to the form-finding problem of cable dome structures.

Although the fundamental analytical theories of cable domes are relatively mature, their analysis still heavily relies on commercial finite element software, resulting in a somewhat cumbersome modeling process. Similar to long-span spatial grid structures, the spatial grid structure design software MSTCAD developed by Luo et al. [7] has wide applicability, ease of operation, and reliability, providing significant assistance and promotion for engineering applications. In light of this, based on the existing static and dynamic analysis methods for tensegrity structures, this paper introduces a specialized modeling and analysis platform for cable dome structures. This platform comprises three primary modules: pre-processing, computational analysis, and post-processing. The pre-processing module facilitates swift modeling of cable dome structures, definition of material and cross-sectional parameters, establishment of constraints, and application of loads. The computational analysis module can undertake a range of complex analyses, including prestress design, section design, static analysis, modal analysis, and dynamic analysis. Finally, the post-processing module achieves data processing and visualization of computational results, enhancing the overall usability and efficacy of the platform.

## 2. Form-finding method for cable dome structures

### 2.1 Nonlinear equilibrium equations

The equilibrium equation of a tensegrity structure can be generated by the principle of minimum potential energy[8]:

$$\mathbf{K}\mathbf{n} = \mathbf{w} \quad (1)$$

where  $\mathbf{K}$  is the global stiffness matrix,  $\mathbf{w}$  denotes the total external forces vector and  $\mathbf{n}$  is the nodal coordinates vector to present the configuration of the structure:

$$\mathbf{n} = \left[ \mathbf{n}_1^T \ \mathbf{n}_2^T \ \cdots \ \mathbf{n}_n^T \right]^T \quad (2)$$

where vector  $\mathbf{n}_i = [x_i \ y_i \ z_i]^T$  is the i-th node's coordinate, in which  $x_i$ ,  $y_i$ ,  $z_i$  denote the nodal coordinate values along the x-, y-, and z-direction respectively.

As the global stiffness matrix  $\mathbf{K}$  is also related to the nodal coordinate  $\mathbf{n}$ , the equilibrium equation shown in Eq.(1) is a typical nonlinear equation. To solve this equation the tangent stiffness matrix  $\mathbf{K}_T$  needs to be obtained by taking the first derivation of the composite function  $\mathbf{K}\mathbf{n}$  with respect to  $\mathbf{n}$  [9], [10].

$$\mathbf{K}_T = \mathbf{K}_G + \mathbf{K}_E \quad (3)$$

$$\mathbf{K}_G = (\mathbf{C}^T \hat{\mathbf{q}} \mathbf{C}) \otimes \mathbf{I}_3 \quad (4)$$

$$\mathbf{K}_E = \mathbf{A}_q \hat{\mathbf{E}} \hat{\mathbf{A}}^{-3} \mathbf{A}_q^T \quad (5)$$

where  $\mathbf{K}_G$  denotes the geometric stiffness,  $\mathbf{K}_E$  denotes the material stiffness.  $\mathbf{I}_3$  is the three-dimensional identity matrix,  $\otimes$  denotes the Kronecker product and  $\mathbf{A}_q$  is the equilibrium matrix with force density  $\mathbf{q}$  as the variable [11].

The geometric stiffness matrix  $\mathbf{K}_g$  of the structure is only related to the topology of the structure  $\mathbf{C}$  and the force density  $\mathbf{q}$  of the elements, while the material stiffness matrix  $\mathbf{K}_E$  is related to topology  $\mathbf{C}$ , nodal coordinates  $\mathbf{n}$ , elements length vector  $\mathbf{l}$ , cross-sectional vector  $\mathbf{A}$  and elastic modulus vector  $\mathbf{E}$ .

## 2.2 Nonlinear least-squares problems

To solve the nonlinear equilibrium equations one of the effective methods is to transform it into nonlinear least-squares problems:

$$\min F(\mathbf{n}) = \frac{1}{2} \sum_{i=1}^{3n} p_i^2(\mathbf{n}) = \frac{1}{2} \mathbf{p}(\mathbf{n})^T \mathbf{p}(\mathbf{n}) \quad (6)$$

where  $p_i$  denotes the unbalanced force on the  $i$ -th node. As the function value approaches zero, it can be inferred that the structure has achieved a state of equilibrium, indicating that the form-finding process is completed. For cable dome structures, we only need to use the unbalanced force on free nodes to construct the nonlinear least squares problems:

$$\min F(\mathbf{n}_f) = \frac{1}{2} \sum_{i=1}^{3n} p_i^2(\mathbf{n}_f) = \frac{1}{2} \mathbf{p}(\mathbf{n}_f)^T \mathbf{p}(\mathbf{n}_f) \quad (7)$$

where  $\mathbf{n}_f$  denotes the free nodes without constraints.

The derivatives of  $F(\mathbf{n})$  can be expressed in terms of the Jacobian matrix  $\mathbf{J}(\mathbf{n})$  and the Hessian matrix  $\mathbf{H}(\mathbf{n})$ :

$$\mathbf{J}(\mathbf{n}) = \left[ \frac{\partial \mathbf{p}(\mathbf{n})}{\partial \mathbf{n}} \right]^T \quad (8)$$

$$\mathbf{H}(\mathbf{n}) = \mathbf{J}(\mathbf{n})^T \mathbf{J}(\mathbf{n}) + \sum_{i=1}^{3n} p_i(\mathbf{n}) \frac{\partial^2 p_i(\mathbf{n})}{\partial^2 \mathbf{n}} = \nabla^2 F(\mathbf{n}) \quad (9)$$

Then, the gradient of  $F(\mathbf{n})$  can be expressed:

$$\nabla F(\mathbf{n}) = \mathbf{J}(\mathbf{n})^T \mathbf{p}(\mathbf{n}) \quad (10)$$

## 2.3 Innovative form-finding method

The nonlinear least-squares problems can be solved by the dog-leg method. In which the iterative step  $\mathbf{h}_{dl}$  can be defined as a combination of the steepest descent direction  $\mathbf{h}_{sd}$  and the Gauss-Newton direction  $\mathbf{h}_{gn}$ :

$$\mathbf{h}_{sd} = -\alpha \nabla F(\mathbf{n}) \quad (11)$$

where  $\alpha$  denotes the coefficient that the steepest descent method could achieve the maximum decrease in the direction of  $-\nabla F(\mathbf{n})$ .

Different from solving the standard Newton equations  $\nabla^2 F(\mathbf{n}) \mathbf{h}_n = -\nabla F(\mathbf{n})$ , the second order term is excluded from  $\nabla^2 F(\mathbf{n})$  and the Gauss-Newton direction is obtained by solving:

$$\mathbf{J}(\mathbf{n})^T \mathbf{J}(\mathbf{n}) \mathbf{h}_{gn} = -\mathbf{J}(\mathbf{n})^T \mathbf{p}(\mathbf{n}) \quad (12)$$

In dog-leg method, it employs a trust region approach to find the relationship between the direction  $\mathbf{h}_{sd}$ ,  $\mathbf{h}_{gn}$  and trust region  $\Delta$ :

$$\mathbf{h}_{dl} = \begin{cases} \mathbf{h}_{gn}, & \text{if } \|\mathbf{h}_{gn}\| \leq \Delta \\ \frac{\Delta}{\|\mathbf{h}_{sd}\|} \mathbf{h}_{sd}, & \text{elseif } \|\alpha \mathbf{h}_{sd}\| \geq \Delta \\ \alpha \mathbf{h}_{sd} + \beta (\mathbf{h}_{gn} - \alpha \mathbf{h}_{sd}), & \text{otherwise} \\ \text{(comput } \beta \text{ such that } \|\mathbf{h}_{dl}\| = \Delta) \end{cases} \quad (13)$$

where trust region  $\Delta$  is a region around the current point in the parameter space, within which the approximation model is considered accurate enough to guide the algorithm. Fig.1 shows the method to determine the iterative step  $\mathbf{h}_{dl}$ :

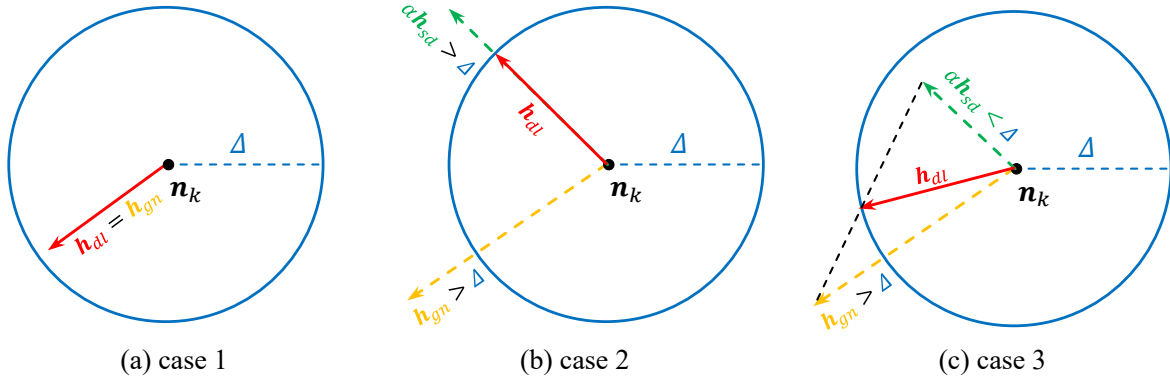


Fig 1 Relationship between the Dog-Leg direction and trust region.

Moreover, the size of the trust region  $\Delta$  is adjusted adaptively during the optimization process to balance the model accuracy and exploration of the parameter space. Here, we use the gain ratio  $\rho$ , which is the ratio of the actual reduction in the objective function to the predicted reduction based on the linear approximation of the objective function, to adjust the size of the trust region adaptively:

$$\rho = \frac{F(\mathbf{n} + \mathbf{h}_{dl}) - F(\mathbf{n})}{\mathbf{h}_{dl}^T \nabla F(\mathbf{n}) + \frac{1}{2} \mathbf{h}_{dl}^T \mathbf{J}(\mathbf{n})^T \mathbf{J}(\mathbf{n}) \mathbf{h}_{dl}} \quad (14)$$

$$\Delta_{k+1} = \begin{cases} \max(\Delta_k, 3\|\mathbf{h}_{dl}\|), & \text{when } \rho \geq 0.75 \\ \Delta_k, & \text{when } 0.25 \leq \rho < 0.75 \\ \Delta_k / 2, & \text{when } \rho < 0.25 \end{cases} \quad (15)$$

It should be noted that the nodal coordinates are only updated for iterative calculation when the gain ratio  $\rho$  is positive.

Notably, when the columns of  $\mathbf{J}(\mathbf{n})$  are linearly related,  $\mathbf{J}(\mathbf{n})^T \mathbf{J}(\mathbf{n})$  becomes singular [12]. As a result, Eq. (12) cannot be solved directly, ultimately leading to the invalidity of the Dog-Leg method. Inevitably, this issue may happen during the form-finding process of the tensegrity structures due to the presence of mechanism displacement modes. To overcome this, the MBFGS (Modified Broyden-Fletcher-Goldfarb-Shanno) method [6] is introduced.

In the MBFGS method, an approximate positive definite matrix  $\mathbf{B}$  is proposed to replace the Hessian matrix during the iteration process. The basic strategy is defined by:

$$\mathbf{B}_{k+1}\mathbf{s}_k = \mathbf{y}_k = \boldsymbol{\delta}_k + \mathbf{v}_k\mathbf{s}_k \quad (16)$$

where  $\mathbf{B}_{k+1}$  denotes the updated  $\mathbf{B}$  matrix,  $\mathbf{s}_k = \mathbf{n}_{k+1} - \mathbf{n}_k$ ,  $\boldsymbol{\delta}_k = \nabla F(\mathbf{n}_{k+1}) - \nabla F(\mathbf{n}_k)$  and  $\mathbf{v}_k = (1 + \max\{-\boldsymbol{\delta}_k^T \mathbf{s}_k / \|\mathbf{s}_k\|^2, 0\}) \cdot \|\nabla F(\mathbf{n}_k)\|$  is a positive constant. Through this strategy, if  $\mathbf{B}_k$  is a positive definite matrix,  $\mathbf{B}_{k+1}$  is ensured to be a positive definite matrix:

$$\mathbf{B}_{k+1} = \mathbf{B}_k - \frac{\mathbf{B}_k \mathbf{s}_k \mathbf{s}_k^T \mathbf{B}_k}{\mathbf{s}_k^T \mathbf{B}_k \mathbf{s}_k} + \frac{\mathbf{y}_k \mathbf{y}_k^T}{\mathbf{y}_k^T \mathbf{s}_k} \quad (17)$$

Based on the MBFGS method, Eq. (12) can be rewritten as:

$$\mathbf{B} \mathbf{h}_{mbfgs} = -\mathbf{J}(\mathbf{n})^T \mathbf{p}(\mathbf{n}) \quad (18)$$

The matrix update strategy in the MBFGS method can gradually approach the Hessian matrix while ensuring the positive definiteness of the  $\mathbf{B}$  matrix. Although it can address the issue of the singularity of  $\mathbf{J}(\mathbf{n})^T \mathbf{J}(\mathbf{n})$ , the MBFGS method comes with a high computational complexity and requires the storage of historical calculation information.

Considering the strengths and weaknesses of both methods, a DL-MBFGS form-finding method is proposed in this paper. The improved Dog-Leg method combines the characteristics of the MBFGS method to replace the Hessian matrix with an updated  $\mathbf{B}$  matrix when  $\mathbf{J}(\mathbf{n})^T \mathbf{J}(\mathbf{n})$  becomes singular. The iterative calculation begins with the Dog-Leg method. During the process, the condition number of  $\mathbf{J}(\mathbf{n})^T \mathbf{J}(\mathbf{n})$  is used to determine whether the Hessian matrix is approaching singularity. If the following equation is satisfied, Eq. (17) is then employed to replace the Hessian matrix:

$$rcond(\mathbf{J}(\mathbf{n})^T \mathbf{J}(\mathbf{n})) < \varepsilon_2 \quad (19)$$

The DL-MBFGS method includes the following main steps.

- (1) Input: initial configuration  $\mathbf{n}_1$ , connectivity matrix  $\mathbf{C}$ , and cross-sectional vector  $\mathbf{A}$ , mass vector  $\mathbf{m}$ , elastic modulus vector  $\mathbf{E}$ , rest length vector  $\mathbf{l}_0$  of all elements.

Set: tolerance of the step size  $\varepsilon_1, \varepsilon_2$ , trust region  $\Delta_1$ .

If  $rcond(\mathbf{J}(\mathbf{n}_0)^T \mathbf{J}(\mathbf{n}_0)) < \varepsilon_2$ , set:  $\mathbf{B}_1 = \mathbf{J}(\mathbf{n}_0)^T \mathbf{J}(\mathbf{n}_0) + 0.1\mathbf{I}$ , where  $\mathbf{I}$  is the identity matrix

- (2) Calculate  $\mathbf{p}(\mathbf{n})$ ,  $F(\mathbf{n})$ ,  $\mathbf{J}(\mathbf{n})$
- (3) Calculate  $\nabla F(\mathbf{n}) = \mathbf{J}(\mathbf{n})^T \mathbf{p}(\mathbf{n})$   
Calculate  $\nabla^2 F(\mathbf{n}) = \mathbf{J}(\mathbf{n})^T \mathbf{J}(\mathbf{n})$
- (4) Judge  $rcond(\mathbf{J}(\mathbf{n})^T \mathbf{J}(\mathbf{n})) < \varepsilon_2$ , if satisfied, calculate Eq. (17), set  $\nabla^2 F(\mathbf{n}) = \mathbf{B}_{k+1}$
- (5) Calculate  $\mathbf{h}_{gn} = -\nabla^2 F(\mathbf{n})^{-1} \nabla F(\mathbf{n})$ , if  $\|\mathbf{h}_{gn}\| \leq \Delta$ ,  $\mathbf{h}_{dl} = \mathbf{h}_{gn}$ ; otherwise, calculate  $\mathbf{h}_{sd} = -\nabla F(\mathbf{n})$ , if  $\|\alpha \mathbf{h}_{sd}\| \geq \Delta$ ,  $\mathbf{h}_{dl} = \frac{\Delta}{\|\mathbf{h}_{sd}\|} \mathbf{h}_{sd}$ , if not  $\mathbf{h}_{dl} = \alpha \mathbf{h}_{sd} + \beta(\mathbf{h}_{gn} - \alpha \mathbf{h}_{sd})$
- (6) Judge the terminal condition  $\|\mathbf{h}_{dl}\| \leq \varepsilon_1$ , and if satisfied, terminate the iteration; if not, go to (7)
- (7) Calculate the gain ratio  $\rho$ , if  $\rho < 0$ , set  $\Delta = \Delta/2$  and go back to (5); otherwise, set  $\mathbf{n} = \mathbf{n} + \mathbf{h}_{dl}$ , meanwhile, if  $\rho \geq 0.75$ , set  $\Delta = \max(\Delta, 3\|\mathbf{h}_{dl}\|)$ , if  $0 \leq \rho < 0.25$ , set  $\Delta = \Delta/2$ ; and go back to (2)

### 3. Modeling and analyzing platform for cable dome structures

The modeling and analyzing platform for the cable dome structure is divided into three modules: the pre-processing module, the computational module, and the post-processing module. The main framework of the program is shown in Fig 2.

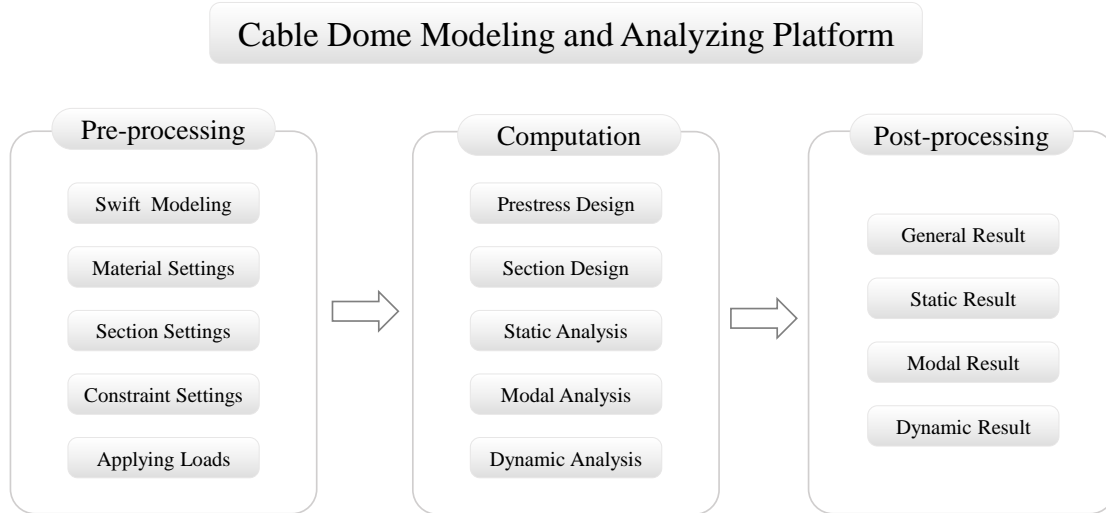


Fig 2 Framework of the platform

#### 3.1 Modeling

The main interface of the platform is shown in Fig 3. Due to the multiple nodes and complex elements, the modeling process of cable dome structures using general finite element software is relatively complex. However, cable dome structures usually have high symmetric geometric configurations and fixed topology characteristics. Based on these characteristics, the pre-processing module of the program provides a parameterized modeling approach. Users only need to select the desired cable dome type (currently available in three forms: Geiger dome, Levy dome, and Geiger-Levy dome), and input parameters such as the span  $S$ , inner ring radius  $Ir$ , rise  $H$ , diagonal cable angle  $\theta$ , circular grids number  $n_c$  and radial grids number  $n_d$  of the designed cable dome. The program can automatically generate the corresponding cable dome structure.

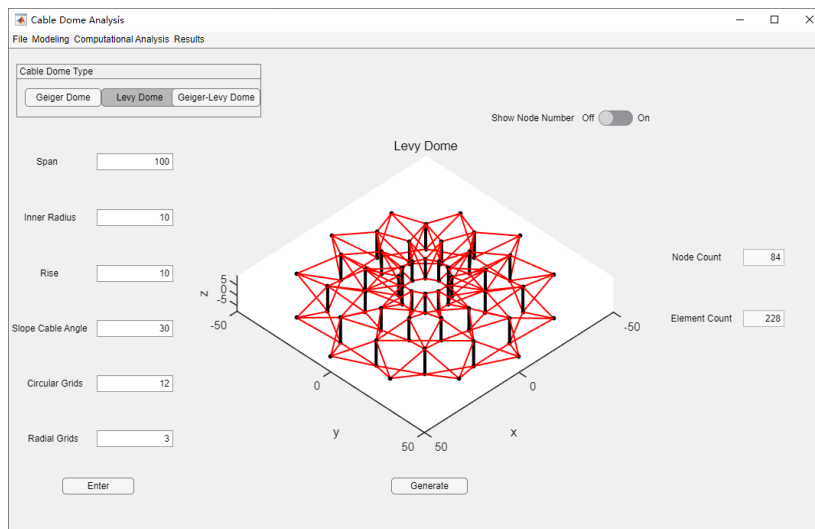


Fig 3 Main interface of the platform

Following the framework, after swift modeling, the pre-processing stage can be finalized by defining the material and section-types, setting boundary constraints and applying external loads.

### 3.2 Analyzing

The computational analysis module serves as the core component of the platform, consolidating a range of classic static and dynamic algorithms. This module encompasses five key sections: prestressed design, section design, static analysis, modal analysis, and dynamic analysis.

In the static analysis section of the software, three methods are integrated: the DL-MBFGS form-finding method proposed in this paper, the modified Newton method [13], and the LMFF method [14]. Each of these methods has their own advantages and can be used to cross-validate the accuracy of the calculation results.

Upon completion of the modeling and calculation analysis of the structure, the software provides a post-processing module for visually presenting the calculation results. This allows designers to gain a clear understanding of the structural performance and facilitates the implementation of corresponding optimization design processes.

### 3.3 Illustrative examples

To further exemplify the efficacy of the DL-MBFGS form-finding method and the cable dome platform, we present an example of a three-dimensional Levy dome.

Consider the Levy dome shown in Fig 4, with a span of 100m, an inner ring radius of 10m, a rise of 10m, and a diagonal cable angle of 30 degrees. The circular grids number is 12 and radial grids number is 3, with a total of 84 nodes and 228 members. The basic unit of the structure is shown in Fig 5, where black lines represent bars and red lines represent cables. Corresponding node and element indexes are marked on each node and element. The overall structure can be obtained by rotating the basic unit around the z-axis at an angle of  $\pi/6$  radians. In the main interface shown in Fig 3, after clicking the generate button, the software will automatically generate the node coordinates and topology of the structure. The initial coordinates of the nodes within the basic unit are listed in Table 1. The group indexes corresponding to each element are shown in Table 2.

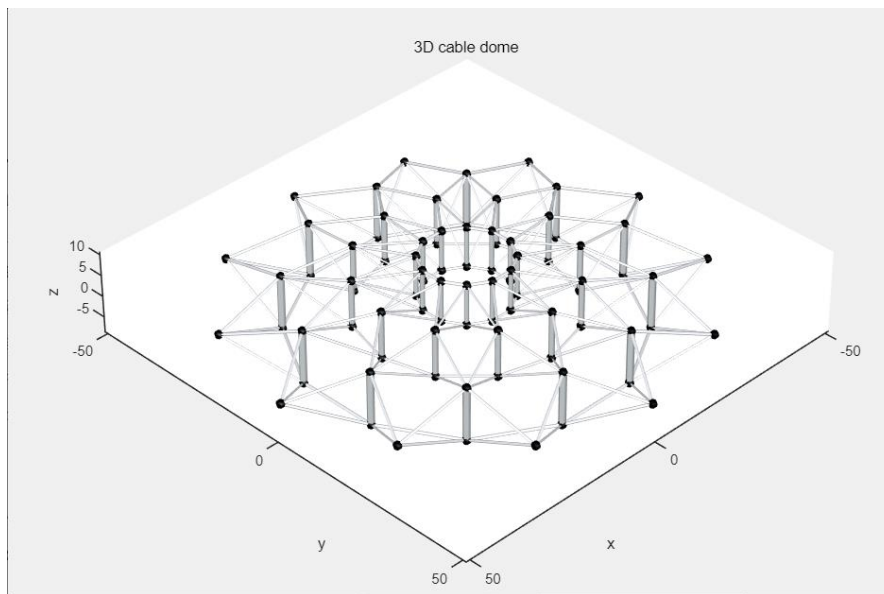


Fig 4 Configuration of Levy dome

Table 1 Initial nodal coordinates of nodes 1 to 7 (unit: m)

Node	1	2	3	4	5	6	7
$x_0$	-35.47	-23.33	-9.66	-35.42	-23.33	-9.66	-50.00
$y_0$	-9.49	0.00	-2.59	-9.49	0.00	-2.59	0.00
$z_0$	4.72	7.89	9.61	-7.70	-2.98	0.19	0.00

Element index	1	2	3	4	5	6	7	8	9	10
Group index	1	2	3	4	4	5	5	6	7	7
Element index	11	12	13	14	15	16	17	18	19	
Group index	8	8	9	10	10	11	11	12	13	

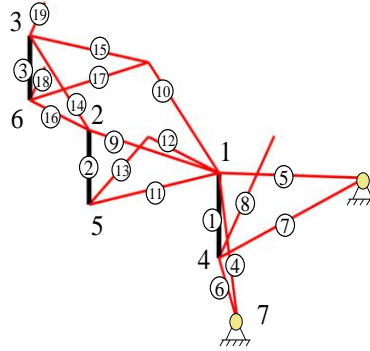


Fig 5 Basic unit of Levy dome

To specify the corresponding material parameters, the Young's modulus of bars and cables are set to be  $2.06 \times 10^{11} Pa$  and  $7.6 \times 10^{10} Pa$  respectively. After prestress and section design, Table 3 and Table 4 present the initial force density and cross-sectional areas of the elements belonging to the  $i$ -th group.

Table 3 Initial force density of the elements comprising the Levy dome

	$q_{01}^g$	$q_{02}^g$	$q_{03}^g$	$q_{04}^g$	$q_{05}^g$	$q_{06}^g$	$q_{07}^g$
Force density ( $N/m$ )	-15455	-69105	-3134	20326	12468	29516	11854
	$q_{08}^g$	$q_{09}^g$	$q_{010}^g$	$q_{011}^g$	$q_{012}^g$	$q_{013}^g$	
Force density ( $N/m$ )	4877	18851	8557	1919	17955	80083	

Table 4 Cross-sectional areas of the elements comprising the Levy dome

	$A_1^g$	$A_2^g$	$A_3^g$	$A_4^g$	$A_5^g$	$A_6^g$	$A_7^g$
Cross-sectional areas ( $mm^2$ )	19130	10466	5694	998	646	1526	507
	$A_8^g$	$A_9^g$	$A_{10}^g$	$A_{11}^g$	$A_{12}^g$	$A_{13}^g$	
Cross-sectional areas ( $mm^2$ )	228	620	327	83	253	1129	

In this case, a surface load of  $800 N/m^2$  is assumed to be applied on the Levy dome. The nodal loads are then calculated based on the projected area, shown in Fig 6.

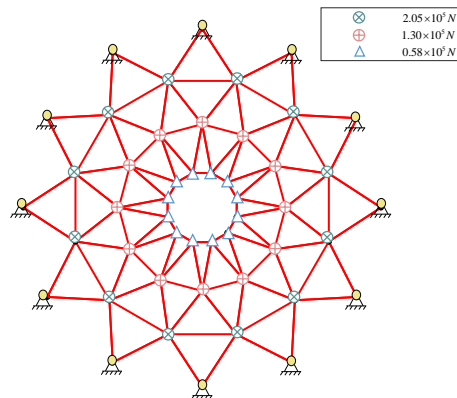


Fig 6 External vertical loads applied on the top nodes.



Considering the slack of cables, the DL-MBFGS method integrated in the platform is then employed to obtain the equilibrium configuration.

Furthermore, we evaluate the accuracy and efficiency of the DL-MBFGS method by comparing the result of the modified Newton method [13] and the LMFF method [15]. Fig 7 (a) shows the z-direction displacement values of Node 1 and Node 2, obtained through the application of the three distinct methods, across a range of surface loading conditions. While Fig 7 (b) illustrates the variations in force density of Element 1 and Element 2 under different surface loading conditions. We can see that the results obtained from the three different methods demonstrate a remarkable level of agreement, providing strong evidence for the accuracy and validity of the DL-MBFG method.

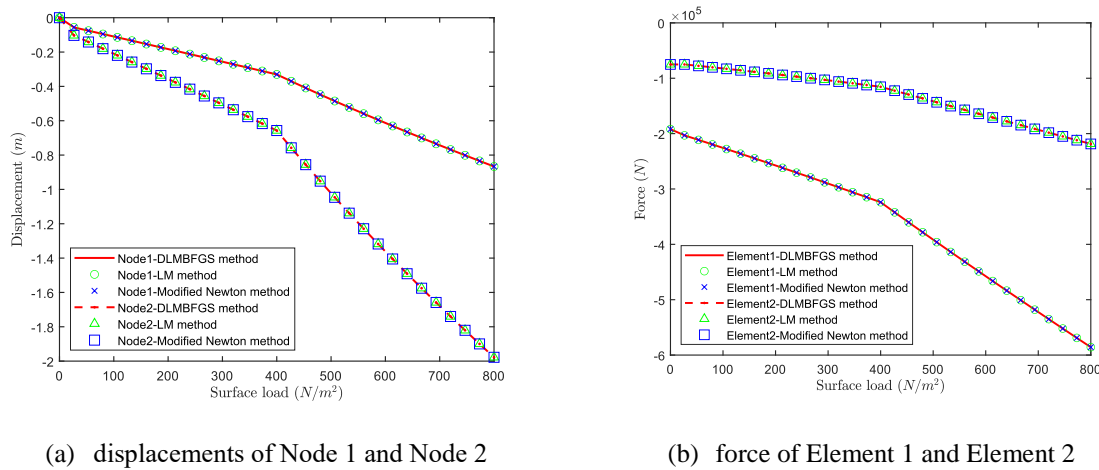


Fig 7 Comparison of results obtained using different methods

To observe the overall stress situation of the structure, the axial force and stress cloud map generated by the software are shown in Fig 8.

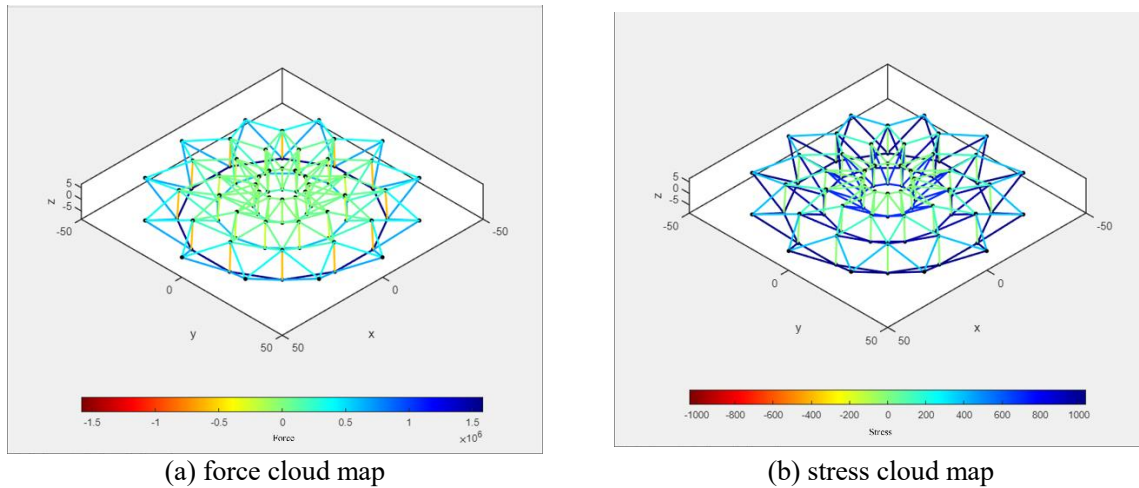


Fig 8 Static cloud map

#### 4. Conclusion

This paper introduces an innovative form-finding method and modeling platform designed for cable dome structures. Adhering to the principles of parametric modeling, users are required to input only a few design parameters to generate the cable dome structure. Serving as the core component of the platform, the computational analysis module, equipped with the DL-MBFGS form-finding method proposed in this article, ensures efficiency and reliability. Concurrently, the platform's post-processing module provides users with a comprehensive overview of calculation results, thereby fostering a deeper understanding of structural performance.

## References

- [1] D. H. Geiger, A. Stefaniuk, and D. Chen, “The design and construction of two cable domes for the Korean Olympics,” in *In: Shells, membranes and space frames. Proceedings of IASS symposium*, Osaka, Japan: Elsevier, 1986, pp. 265–272.
- [2] D. H. Geiger, “Design details of an elliptical cable dome and a large span cable dome (210 m) under construction in the United States,” in *Proc., IASS ASCE. Int. Symp. on Innovative Applications of Shells and Spatial Forms*, Oxford, UK: Oxford Univ. Press, 1988.
- [3] M. P. Levy, “The Georgia Dome and beyond: achieving lightweight-longspan structures,” in *In: Spatial, lattice and tension structures. Proceedings of IASS-ASCE international symposium*, New York: ASCE, 1994, pp. 560–562.
- [4] M. Schenk, S. D. Guest, and J. L. Herder, “Zero stiffness tensegrity structures,” *International Journal of Solids and Structures*, vol. 44, no. 20, pp. 6569–6583, 2007.
- [5] J. Nocedal and S. J. Wright, *Numerical optimization*. Springer, 1999.
- [6] D.-H. Li and M. Fukushima, “A modified BFGS method and its global convergence in nonconvex minimization,” *J Comput Appl Math*, vol. 129, no. 1, pp. 15–35, 2001.
- [7] Y. Z. Luo and S. L. Dong, “Developing of the microcomputer design software MSTCAD for space grid structures,” *Spatial Structures (in Chinese)*, vol. 1, no. 3, pp. 53–59, 1995.
- [8] Y. Zhou, Y. Wang, S. Li, C. Yang, and Y. Luo, “An improved dog-leg method for form-finding of tensegrity structures,” *Computers & Structures*, vol. 292, p. 107237, Feb. 2024.
- [9] S. D. Guest, “The stiffness of tensegrity structures,” *IMA J Appl Math.*, vol. 76, no. 1, pp. 57–66, Dec. 2010.
- [10] S. Guest, “The stiffness of prestressed frameworks: A unifying approach,” *Int. J. Solids Struct.*, vol. 43, no. 3, pp. 842–854, 2006.
- [11] S. Pellegrino and C. R. Calladine, “Matrix analysis of statically and kinematically indeterminate frameworks,” *Int J Solids Struct.*, vol. 22, no. 4, pp. 409–428, 1986.
- [12] C. D. Meyer, *Matrix analysis and applied linear algebra*, vol. 188. Siam, 2023.
- [13] S. Ma, X. Yuan, and S. Xie, “A New Genetic Algorithm-based Topology Optimization Method of Tensegrity Tori,” *KSCE J. Civ. Eng.*, vol. 23, no. 5, pp. 2136–2147, May 2019.
- [14] Y. Wang, X. Xu, and Y. Luo, “Form-finding of tensegrity structures via rank minimization of force density matrix,” *Engineering Structures*, vol. 227, p. 111419, Jan. 2021.
- [15] X.-F. Yuan, S. Ma, and S.-H. Jiang, “Form-finding of tensegrity structures based on the Levenberg–Marquardt method,” *Comput. Struct.*, vol. 192, pp. 171–180, 2017.



*Proceedings of the IASS 2024 Symposium  
Redefining the Art of Structural Design  
August 26-30, 2024, Zurich Switzerland  
Philippe Block, Giulia Boller, Catherine De Wolf,  
Jacqueline Pauli, Walter Kaufmann (eds.)*

---

## Copyright Declaration

Before publication of your paper in the Proceedings of the IASS Annual Symposium 2024, the Editors and the IASS Secretariat must receive a signed Copyright Declaration. The completed and signed declaration may be uploaded to the EasyChair submission platform or sent as an e-mail attachment to the symposium secretariat ([papers@iass2024.org](mailto:papers@iass2024.org)). A scan into a .pdf file of the signed declaration is acceptable in lieu of the signed original. In the case of a contribution by multiple authors, either the corresponding author or an author who has the authority to represent all the other authors should provide his or her address, phone and E-mail and sign the declaration.

Paper Title: Innovative form-finding method and modeling platform for cable dome design

Author(s): Yan Zhou, Mingzhe Ma, Yaozhi Luo

Affiliation(s): College of Civil Engineering and Architecture, Zhejiang University

Address: An-zhong Building, 866 Yuhangtang Road, Hangzhou, China

Phone: +86-13865272051

E-mail: [zhouyan98@zju.edu.cn](mailto:zhouyan98@zju.edu.cn)


---

I hereby license the International Association for Shell and Spatial Structures to publish this work and to use it for all current and future print and electronic issues of the Proceedings of the IASS Annual Symposia. I understand this licence does not restrict any of the authors' future use or reproduction of the contents of this work. I also understand that the first-page footer of the manuscript is to bear the appropriately completed notation:

*Copyright © 2024 by <name(s) of all of the author(s)>  
Published by the International Association for Shell and Spatial Structures (IASS) with permission*

If the contribution contains materials bearing a copyright by others, I further affirm that (1) the authors have secured and retained formal permission to reproduce such materials, and (2) any and all such materials are properly acknowledged by reference citations and/or with credits in the captions of photos/figures/tables.

Printed name: Yan Zhou

Signature: 

Location: Hangzhou, China

Date: 2024.5.25